A method for detecting bubbles in two-phase gas-liquid flow

P. Hanafizadeh*, A. Sattari, S. E. Hosseinidoost, M. Molaei and M. Ashjaee

Center of Excellence in Design and Optimization of Energy Systems, School of Mechanical Engineering, College of Engineering, University of Tehran, Tehran, Iran

Abstract

Bubble detecting bubble has been a basic issue in two-phase flow systems. In this paper, a new method for measuring the frequency of bubble formation is presented. For this purpose, an electronic device is designed and constructed to work based on a change in intensity of the laser beam. Continues light beam is embedded just above the needle, which is received by a phototransistor. When bubbles go through the light beam, they make a deviation on it and change its intensity. So, the electrical resistance between two bases of phototransistor changes, and this variation is sensed by an electronic board. Based on the number of interruption and duration time, the frequency of bubble formation is be calculated. Liquid and gas phases in the present work are water and air, respectively. Tests are performed in constant liquid height (60 mm above the needle), constant needle diameter (1.6 mm), and gas flow rates between 50 to 1200 ml/hr. Also, three other methods are utilized to measure the bubble frequency: image processing (IP), numerical modeling, and theoretical model. Results show that with an increase in the flow rate of the gas phase, the frequency of formation increases approximately in a linear manner. Validation of methods with IP method shows that the new device has very good accuracy for measuring bubble formation frequency. So because of the simplicity of using and low cost, it can be a superseded method of image processing.

Nomenclature

a	Acceleration		u	Velocity
A	Projection area of bubble		U_f	Volume flux through the face
D	Diameter of bubble		V	Volume of bubble
f	Frequency of bubble formation		V_C	Volume of cell
F_B	Buoyancy force		*Greek symbols*	
F_D	Drag force		α_q	Volume fraction
F_V	Virtual mass force		θ	Contact angle of bubble
F_σ	Surface tension force		ρ	Density
G	Gravity force		σ	Interfacial tension
m	Bubble mass		*Subscripts*	
$\dot{m}$	Mass transfer		g	Gas phase
P	Circumference of the needle		l	Liquid phase
Q	Volumetric flow rate		p	Phase p
Re	Reynolds number		q	Phase q

*Corresponding author
Email address: hanafizadeh@ut.ac.ir

1. Introduction

The dynamic of bubble formation has a major role in diverse applications related to scattering of gas bubbles in liquids such as water treatment, chemical reactors, metallurgy, and medical. Also, it is an important subject in the context of two-phase heat transfer [1-3]. This phenomenon is affected by different parameters such as the equivalent diameter of injection, the geometry of injection, gas flow rate, liquid and gas physical properties, the height of the liquid column, and wettability.

On the terrain of bubble formation in various conditions, abundant works have been done. For instance, Davidson and Amick [4] worked on the formation of gas bubbles at horizontal orifices. Influence of different parameters was examined on the formation of bubbles such as the diameter of the orifice, the volume of the chamber, and physical properties. In another research, Ramakrishnan et al. [5] studied bubble formation under constant flow conditions and proposed a model based on two-step mechanism of bubble formation. Also, Akita and Yoshida [6] investigated bubble size, interfacial area, and liquid-phase mass transfer coefficient in bubble columns. They presented dimensionless correlations for the average bubble size. In another paper, Sada et al. [7] conducted a research on bubble formation in a flowing liquid. They found that the bubble size in the flowing liquid decreases with increasing superficial liquid velocity and decreasing gas flow rate. Furthermore, Tsuge and Hibino [8] investigated bubble formation from an orifice submerged in liquids. The effects of various factors, such as orifice diameter, gas physical properties and gas chamber on the volume of bubbles were explored. Also, Kim et al. [9] developed a theoretical model for bubble and drop formation in flowing liquids in microgravity using a force balance. They found that the bubbles are detached from the nozzle only by the liquid flow drag. Byakova et al. [10] examined the influence of wetting conditions on bubble formation at the orifice in an inviscid liquid mechanism of bubble evolution. They concluded that the influence of operating variables on the formation of the bubble is different under various wetting conditions. Corchero et al. [11] performed experimental investigations on the effects of wetting conditions and flow rate on bubble formation at orifices. Also, a simple model of the bubble shape at detachment was proposed that gives results in good agreement with those obtained from experiments done at small flow rates. Qu and Qiu [12] worked on bubble dynamics under a horizontal microheater array. They studied the effects of Marangoni, buoyancy, and drag forces on the bubble dynamic phenomena using experimental data. In another work, Ohta et al. [13] conducted a computational study on the dynamic motion of a bubble rising in Carreau model fluids. They utilized the Volume of Fluid (VOF) numerical model in order to simulate the mechanism of bubble formation. They discussed bubble rise motion in shear-thinning fluids in terms of the effective viscosity, and the effective Reynolds and Morton numbers. In another work, Vafaei et al. [14] investigated the bubble growth rate from needle nozzles. They realized that the bubble volume expansion rate follows a cyclic behavior for the substrate nozzles while it shows a smooth decrease after an initial increase for the needle nozzles. Finally, Di Bari and Robinson [15] conducted an experimental study of gas injected bubble growth from submerged orifices. The quasi-static growth and departure characteristics showed little dependence on the growth rate while having a notable dependence on the orifice size.

Among the parameters influencing the formation of bubbles, the frequency of bubble formation and its relationship with gas flow rate are the major issues for bubble formation, which have been attracted many attentions in the literature. Almost in all investigations, it is found that the bubble frequency increases with increasing gas flow rate [16–20]. Most researchers utilized a high-speed camera and image processing (IP) method to compute frequency of bubble formation which has high cost and time-consuming. Also, in industrial applications of bubble formation, the image processing cannot be used because of the need to momentary measure the frequency. Some researchers measured the frequency by counting the number of bubbles generated in a specified interval,

although it is not an accurate method nowise. Another method for measuring bubble formation frequency utilized by some researches is the use of different kinds of probes, like optical and conductivity probes, which are high costs as high-speed cameras. For instance, Harvey et al. [21] measured vapor bubble using image analysis. They presented a method of computer image analysis to determine flow quantities of a single vapor bubble as it evolves near a rigid boundary. Also, Davidson et al. [22] measured the frequency of bubble formation by stroboscopic illumination. By experimental investigations, they concluded that the frequency of bubble formation decreases with increasing orifice diameter. In another paper, Lguchi et al. [23] investigated the effects of cross-flow on the frequency of bubble formation from a single-hole nozzle using a high-speed camera. They compared the frequency of bubble formation in a rotating bubble bath with that of a stationary one and concluded that before a critical value of cross-flow velocity, the ratio of frequencies is unity and after that, it changes in a complex manner. In another research, Badam et al. [24] perused regimes of bubble formation experimentally utilizing a high-speed camera. They found that at high gas flow rates, bubble formation frequency remains constant and bubble volume is almost independent of surface tension. Also, Zhang et al. [25] worked on drag coefficient on bubble rising. They calculated the volume of the bubble by dividing the gas flow rate to bubble formation frequency. They measured the frequency of bubble formation by counting the bubbles generated in a time interval. In addition, Hanafizadeh et al. [26–28] in a series of studies investigated the formation, growth, and detachment of gas bubbles produced from a submerged needle in water using a high-speed camera. They concluded that bubble formation frequency strongly depends on the contact angle and the surface tension, and it increases with increasing gas flow rate.

In the current work, a new method for calculating bubble frequency is presented. In this method, an electronic device is designed and constructed to work based on changes in the intensity of the light beam. Also, the frequency is measured using image processing, numerical,

and theoretical methods. Finally, errors of methods are computed in comparison with the IP method (because this technique has been widely used in the literature) and the most accurate method is specified.

2. Experimental apparatus

Schematic view of the experimental setup of the present work is shown in Fig. 1. The experimental system consists of a syringe pump, a square column, a standard circular needle with 1.6 mm diameter, a light source, a high-speed video camera (1200 fps), and a frequency meter device. For photographic observations, the square column made from PMMA with a dimensions of 100 mm × 100 mm × 300 mm and open to the atmosphere at the top is utilized ((1) in Fig. 1). The height of the liquid is constant and equal to 60 mm above the needle. The camera records movies with 1200 fps and 336×96 pixels ((4) in Fig. 1) and sends them to the computer ((6) in Fig. 1) for image processing. In order to wipe out reflections, one 800 W halogen lamp is placed just in front of the camera ((5) in Fig. 1). The injection system located at the bottom of the column is composed of a needle ((2) in Fig. 1) as a source of injection joint to an automatically controlled syringe pump ((3) in Fig. 1). The syringe pump is filled with air, and the flow rate range is between 50 to 1200 ml/hr. The frequency meter system contains a 200 mW laser ((9) in Fig. 1), a phototransistor ((7 in Fig. 1) and an electronic board ((8) in Fig. 1) for processing data. The range of operating conditions are given in Table 1 (physical properties are computed at 20°C).

Table 1. The range of operating conditions.

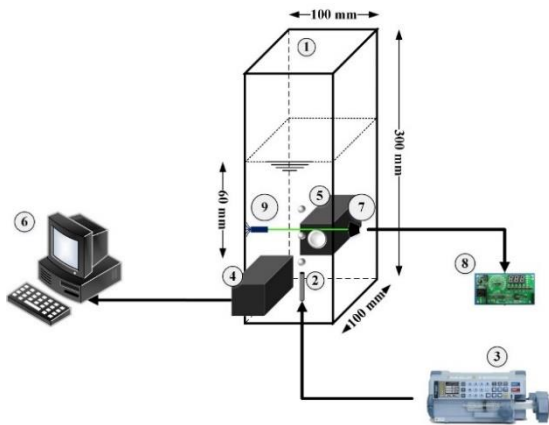| Parameter	value
Flow rate	50-1200 mlph
Needle diameter	1.6 mm
Liquid height	60 mm
Liquid viscosity	0.001 Pa. s
Surface tension	72.5×10^{-3} N. m^{-1}
Water density	997.05 kg. m^{-3}
Air density	1.15 kg. m^{-3}

Fig. 1. Schematic view of the experimental setup; (1) bubble column, (2) injection needle, (3) syringe pump, (4) high-speed video camera, (5) light source, (6) computer, (7) phototransistor, (8) electronic board, and (9) laser.

When the variables are the values of experimental measurements, they have uncertainties due to measurement limitations. For the present research, the uncertainties of measured data are given in Table 2. In this table, based on the accuracy of the measuring instruments, the precision of the major parameters is reported. Moreover, based on the analysis of the uncertainty studied by Lazar et al. [29], the uncertainty of the bubble diameter and volume are computed.

Table 2. The uncertainty of the experimentally measured variables.

| Parameter	Amount of uncertainty	Percentage of uncertainty
Air flow rate	−	3%
Needle diameter	0.005 mm	−
Physical calibration scale	0.005 mm	−
Image calibration scale	1 *pixel*	−
Bubble diameter	0.05 mm	−
Bubble volume	0.1 mm^3	−

3. Methodology

As mentioned before, four methods are utilized in this project to measure the frequency of bubble formation; image processing (IP),

frequency device, numerical modeling, and theoretical model. Each of this methods is explained except the IP method. For the detail of the IP method see Ref. [30].

3.1. Frequency measurement unit

In order to measure the frequency of bubble formation, a continuous light beam is embedded just above the needle, which is received by a phototransistor as shown in Fig. 1. When bubbles go through this light beam, make a deviation on that and change the intensity of light. So, the electrical resistance between two bases of phototransistor changes and this variation is sensed by an electronic board. According to the number of interruption and duration time, the frequency of bubble formation can be calculated. Fig. 2(a) and (b) shows the continuous and interrupted light beam by rising bubble, respectively.
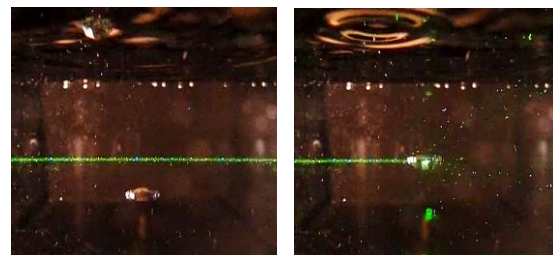

   **(a)**   **(b)**
Fig. 2. (a) Continuous light beam and (b) interrupted light beam by the bubble.

The phototransistor is an analog sensor that its electrical resistance changes with the received intensity of light. To measure this with a microcontroller, the resistance should be converted to voltage in a suitable range. For that reason, a voltage divider is recruited. Voltage divider allows the microcontroller to measure the resistance of the sensor. The sensor is wired in series with a known resistance to form a voltage divider, and a known voltage is applied across the divider. Then the center tap of the divider is connected to microcontroller's analog-to-digital converter and the tap's voltage is measured. Next, by using the known resistance and voltage, the resistance of the sensor can be computed.

Fig. 3 illustrates the measured voltage versus time for different flow rates. The peaks of the charts are related to the moments in which the laser beam is interrupted by rising bubbles. Furthermore, it is clear that with increasing gas flow rate, the distance between peaks gets closer to each other which means the frequency of formation increases. This can be justified by this fact that with increasing gas flow rate, the upward forces acting upon rising bubble dominates downward forces and resulted in a lower time of formation.
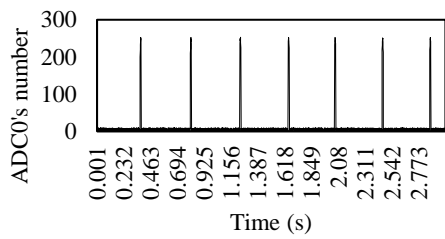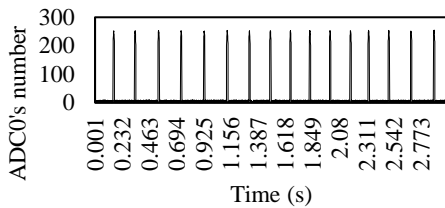

(a)
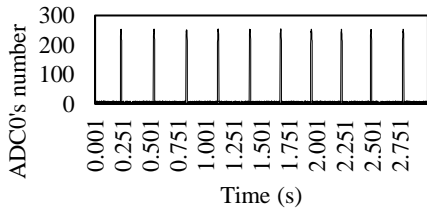
(b)
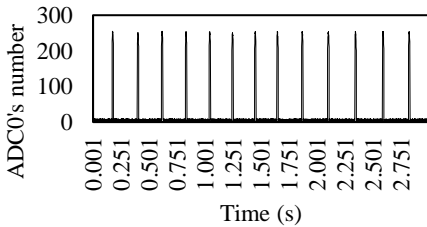
(c)

(d)

Fig. 3. Fluctuation time for (a) 400 (b) 600 (c) 800 (d) 1000 ml/hr flow rate with frequency device.

3.2. Theoretical modeling

To compare the obtained results from the presented method, a theoretical model based on force balancing is also used in this paper. Assumptions of force balancing in the theoretical modeling are as follows:

• All properties of fluids are assumed to be constant and are computed at room temperature.
• Bubble growth happens adiabatically and axisymmetric.
• The liquid is quiescent, so the liquid trust force is not considered.
• The pressure of the gas is uniform within the bubble, and the influence of gas viscosity is negligible due to the high Reynolds number.
• Gas momentum force is negligible compared with other forces acting on the bubble.
• As the thickness of the orifice is negligible, in comparison with the equivalent diameters of it, the contact line between the needle and bubble is considered to be fixed to the inner rim of the needle.

Based on the second law of Newton and the above assumptions, and by considering Fig. 4, the force balance equation can be written as follow:

$$ma = F_B + F_\sigma + F_D + F_V + G \qquad (1)$$

where F_B, F_σ, F_D, F_V, and G are buoyancy, surface tension, drag, virtual mass, and gravity forces, respectively [31]. So force balance can be written as follow:

$$m_g a_y = (\rho_l - \rho_g)gV_g - \sigma P\sin\theta$$
$$-\frac{1}{2}\rho_l C_D u_g^2 A \qquad (2)$$
$$-\frac{1}{2}V_g \rho_l a_y$$

By simplifying the above equation, the final equation for bubble volume is as follow:

$$V_g = \frac{\rho_l C_D u_g^2 A + 2\sigma P\sin\theta}{2(\rho_l - \rho_g)g - (\rho_l + 2\rho_g)a_y} \qquad (3)$$

where:
ρ_l: Density of liquid phase
ρ_g: Density of gas phase

C_D: Drag coefficient (that is dependent on Reynolds number)

u_g: Gas velocity

S: Reference area of the bubble (that is equal to $\pi D^2/4$)

a_y: Acceleration of rising bubble

σ: The surface tension between water and air

θ: Contact angle of the bubble at the detachment

P: Circumference of the injection needle

For Reynolds numbers between 20 and 260, C_D can be calculated by Ishii equation (Eq. (4)) [32]:

$$C_D = \frac{24}{Re}(1 + 0.1Re^{0.75}) \tag{4}$$

Finally, the frequency of bubble formation can easily be computed using the flow rate as below:

$$f = \frac{Q}{V_g}$$
$$= Q \times \frac{2(\rho_l - \rho_g)g - (\rho_l + 2\rho_g)a_y}{\rho_l C_D u_g^2 A + 2\sigma P sin\theta} \tag{5}$$

where Q is the flow rate of the dispersed phase and V_g is the volume of the bubble at the detachment.

In this research, velocity and also its changes are very small at detachment, so drag force and acceleration are negligible. Therefore, Eqs. (3) and (5) are simplified as below:

$$V_g = \frac{2\sigma P sin\theta}{2(\rho_l - \rho_g)g} \tag{6}$$

$$f = \frac{Q}{V_g} = Q \times \frac{2(\rho_l - \rho_g)g}{2\sigma P sin\theta} \tag{7}$$

Q in the above formula is obtained from the syringe pump that plays both roles of injection and controlling flow. ρ_l, ρ_g and σ are physical properties of the liquid and gas phase and are measured at 20°C. P is the circumference of the circular needle that can easily be computed from the below equation:

$$P = \pi D \tag{8}$$

where D is the diameter of the needle. Finally, θ is the contact angle of the bubble at detachment that is computed using experimental data processed by the image processing method. So, a theoretical method is dependent on experimental data due to the contact angle.
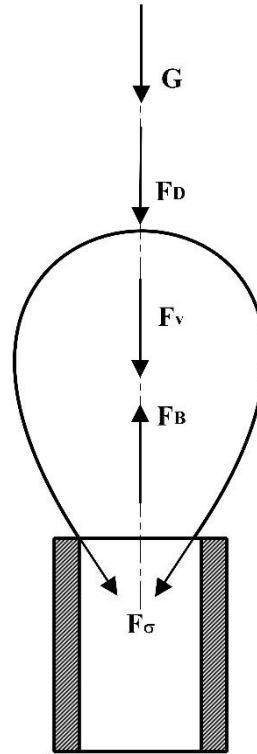

Fig. 4. Schematic force balance in the current study.

3.3. Numerical modeling

In this study, the bubble formation process is simulated by applying the VOF method. The flow is supposed to be Newtonian, and the gas and liquid phases are considered as incompressible fluids. Two or more immiscible fluids can be modeled by the VOF model through solving a single set of momentum equations and exploring the volume fraction of the fluids all over the domain. The VOF formulation is based on not osmosing the two or more fluids (or phases). For each additional phase, the volume fraction of the phase in the computational cell is introduced. The volume fractions of all phases sum up to unity for each control volume. If the qth fluid's volume

fraction in the cell is marked as α_q, then three conditions may happen [33]:

- $\alpha_q = 0$: The cell is empty (of the qth fluid).
- $\alpha_q = 1$: The cell is full (of the qth fluid).
- $0 < \alpha_q < 1$: The cell contains the interface between the qth fluid and one or more other fluids.

Suitable properties and variables are determined for each control volume within the domain based on the local value of α_q.

3.3.1. Volume fraction equation

Exploring the interface(s) between the phases is accomplished by solving the continuity equation for the volume fraction of one (or more) of the phases. For the qth phase, this equation is as follows [33]:

$$\frac{1}{\rho_q}\left[\frac{\partial}{\partial t}\left(\alpha_q \rho_q\right) + \nabla \cdot \left(\alpha_q \rho_q \vec{v}_q\right)\right. $$
$$= S_{\alpha_q} \qquad (9)$$
$$\left. + \sum_{p=1}^{n}\left(\dot{m}_{pq} - \dot{m}_{qp}\right)\right]$$

where $\dot{m}_{pq}$ is the mass transfer from phase q to phase p and $\dot{m}_{pq}$ is the mass transfer from phase p to phase q.

The volume fraction equation is not solved for the primary phase, while the primary-phase volume fraction is computed based on the following constraint [33]:

$$\sum_{q=1}^{n} \alpha_q = 1 \qquad (10)$$

The volume fraction equation can be solved through implicit or explicit time discretization. Because of the faster convergence rate of the explicit method, using this method is preferred in this paper.

3.3.2. The explicit scheme

The formulation of this method can be defined as below [33]:

$$\frac{\alpha_q^{n+1}\rho_q^{n+1} - \alpha_q^n \rho_q^n}{\Delta t}V_c$$
$$+ \sum_f \left(\rho_q U_f^n \alpha_{q,f}^n\right)$$
$$= \left[S_{\alpha_q} \right. \qquad (11)$$
$$\left. + \sum_{p=1}^{n}\left(\dot{m}_{pq} - \dot{m}_{qp}\right)\right]V$$

where $n + 1$ is the index for new (current) time step, n is the index for previous time step, $\alpha_{f,q}$ is the face value of the qth volume fraction, V_c is the volume of the cell, and U_f is the volume flux through the face, based on normal velocity. This formulation does not require the iterative solution of the transport equation during each time step.

3.3.3. Momentum equation

Throughout the domain, a single momentum equation is solved, and the resulting velocity field is shared between the phases. The momentum equation is dependent on the volume fractions of all phases through the properties of ρ and μ as below[33]:

$$\frac{\partial}{\partial t}(\rho\vec{v}) + \nabla.(\rho\vec{v}\vec{v})$$
$$= -\nabla p \qquad (12)$$
$$+ \nabla.\left[\mu(\nabla\vec{v} + \nabla\vec{v}^T)\right]$$
$$+ \rho\vec{g} + \vec{F}$$

It should be noted that both phases in the present study are considered to be incompressible.

In cases with large velocity differences between the phases, the accuracy of the velocities calculated near the interface can be adversely affected, and this is one restriction of the shared-field approximation.

In Fig. 5, bubble formation sequence as a comparison between experimental and numerical methods for 800 ml/hr flow rate can be seen. Generally, the formation of bubble happens in three different stages: weeping, expansion, and detachment. In the first stage, the bubble is not conducted due to the high

contribution of downward forces. In next stage, a bubble is formed with low velocity, so upward and downward forces are approximately. In the final stage, upward forces dominate downward ones, and an acceleration movement happens. Also, as shown in this figure, the numerical method can predict the sequence of the bubble formation pretty well and has a good agreement with the real bubble formation process.
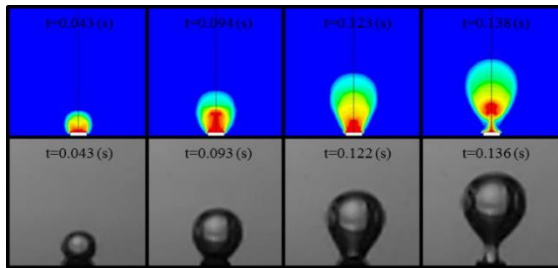

Fig. 5. Comparison of bubble formation sequence between numerical and experimental data for 800 ml/hr flow rate.

In order to calculate the bubble frequency formation using a numerical method, contours of volume fraction are gathered as picture files and then by image processing method, the frequency is computed.

4. Results and discussions

Results are divided into two sections: results of frequency device, as the main approach of the current paper, and those of other methods. In the first section, details of gathering processing data by frequency and the device are explained and presented. In the next section, the results of other methods are just presented.

The results gathered by the frequency device are shown in Fig. 4. As shown in these diagrams, ADC0's number versus time can be seen. By interrupting the light beam by bubbles, the ADC0's number reaches approximately 250. So by the number of peaks in diagrams and duration time of them, the frequency of bubble formation can easily be computed. Also, it is clear from the figure that with increasing gas flow rate, the number of picks in a certain time increasesmeaning that the frequency of formation increases. The results of methods

applied to measure the frequency of formation for different flow rates are shown in Table 3.

Table 2. Comparison of frequency results of different methods.

Flow rate (ml/hr)	Image processing (Hz)	Frequency device (Hz)	Numerical (Hz)	Theoretical (Hz)
50	0.4836	0.4754	0.7097	0.4886
100	1.0093	0.9894	1.4493	0.9491
200	1.8519	1.8186	2.0534	1.7908
400	3.4823	3.4448	3.5714	3.5218
600	5.2131	5.1570	5.6818	5.2570
800	7.0468	6.9655	6.8966	6.9382
1000	8.4906	8.3219	8.8757	8.6539
1200	10.8768	10.6704	10.1371	10.3837

As the IP technique has been widely used in the literature, the obtained results of the other methods are compared with this method. The calculated percentage of errors are tabulated in Table 4. The presented errors are computed according to the following equation:

$$\%Error = \frac{f_{IP} - f_i}{f_{IP}} \times 100 \qquad (13)$$

where f_{IP} and f_i are the frequency of bubble formation measured from the IP and other methods, respectively.

Table 4. Errors of different methods in comparison with the IP method.

Flow rate (ml/hr)	Frequency device (%)	Numerical (%)	Theoretical (%)
50	1.6956	46.7535	1.0339
100	1.9717	43.5946	5.9645
200	1.7982	10.8807	3.2993
400	1.0769	2.5587	1.1343
600	1.0761	8.9908	0.8421
800	1.1537	2.1315	1.5411
1000	1.9869	4.5356	1.9233
1200	1.8976	6.8007	4.5335

As shown in Table 4, the results of frequency device have most accordance with IP. It shows that in spite of the low cost of this device, its accuracy is acceptable. Also, errors of theory model show that in the current range of flow rates (50 to 1200 ml/hr) and present operating conditions, balance of forces can easily be defined as a balance of buoyancy and surface

tension forces. It demonstrates assumptions for deriving Eq. (7) are admissible. Finally, as shown in Table 4, the numerical method has the lowest accuracy, especially at high flow rates, but it is not originated from the actual results so far. One major reason of this low accuracy is the difficulty of modeling the interface of gas and liquid phases in the numerical model due to the numerical diffusion and the need for a high grid resolution, which results in a non-sharp interface.

Fig. 6 shows the frequency of bubble formation versus flow rate for four mentioned methods. As can be seen, the frequency of formation increases approximately linearly with increasing gas flow rate. It can be justified with this fact that increasing gas flow rate tends to the increase in momentum of the bubble. As a result, faster detachment is obtained in higher frequency of formation at higher flow rates. As shown in Fig. 6, the frequency device method has the most precision between two other methods (numerical and theory model). Also, results confirm the previous researches which by increasing the flow rate of gas injection, the frequency of bubble formation increases.
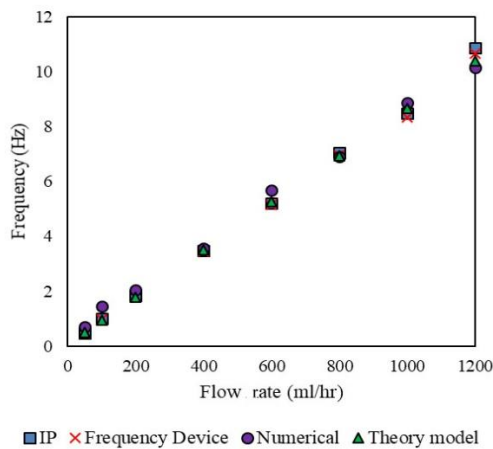

Fig. 6. Frequency of bubble formation versus flow rate for four methods.

Fig. 7 illustrates the diagram of IP versus frequency device method. The average root mean square error between the results of frequency device and image processing method is less than 2% showing that the device has good accuracy.
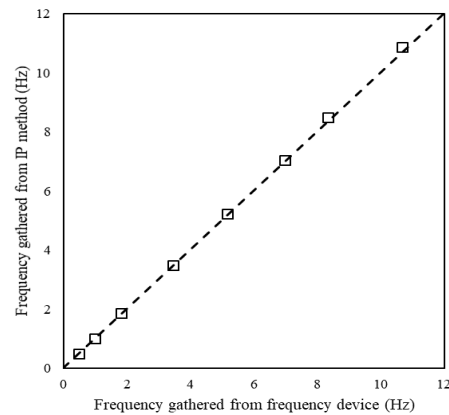

Fig. 7. Frequency of bubble formation from IP method versus frequency device method.

To put the accuracy of this method into perspective, two of the most important correlations presented for calculating the volume of the bubble at the detachment in constant flow condition are taken into account. Then using Eq. (7), the frequency of formation for each correlation is calculated and compared with the experimental data of the present study, and shown in Fig. 8. As can be seen, both correlations presented by Gaddis and Vogelpohl [34] and Jamialahmadi et al. [35] have good agreement with the experimental data, especially at relatively low flow rates. The most error between the experimental data and Gaddis and Vogelpohl correlation is about 14%, while this error for Jamialahmadi et al. correlation is about 18%.
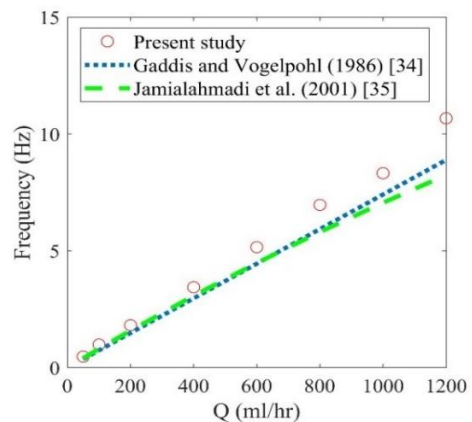

Fig. 8. Prediction of frequency from various correlations and experimental data of the present work.

5. Conclusions

In this paper, an electronic device is designed and constructed to measure the frequency of bubble formation based on a change in intensity of the laser beam. The main features of the device are:

- High accuracy despite the low cost
- The ability of momentary measuring of bubble or any other object frequency for industrial applications
- Simple electronic circuit
- So simple to use

The accuracy of this new method is compared with other common methods: IP, numerical and theoretical modeling. Results show that this method has very good accuracy. The average root mean square error between the results of frequency device and image processing method is less than 2%. So it can be used as an alternative method of image processing in many applications.

References

[1] M. G. Reddy, M. V. V. N. L. S. Rani, K. G. Kumar, and B. C. Prasannakumara, "Cattaneo–Christov heat flux and non-uniform heat-source/sink impacts on radiative Oldroyd-B two-phase flow across a cone/wedge," *J. Brazilian Soc. Mech. Sci. Eng.*, Vol. 40, No. 2, p. 95, (2018).

[2] M. G. Reddy and O. D. Makinde, "Magnetohydrodynamic peristaltic transport of Jeffrey nanofluid in an asymmetric channel," *J. Mol. Liq.*, Vol. 223, pp. 1242-1248, (2016).

[3] M. Gnaneswara Reddy and N. Sandeep, "Free convective heat and mass transfer of magnetic bio-convective flow caused by a rotating cone and plate in the presence of nonlinear thermal radiation and cross diffusion," *J. Comput. Appl. Res. Mech. Eng.*, Vol. 7, No. 1, pp. 1-21, (2017).

[4] L. Davidson and J. Erwin H. Amick, "Formation of Gas Bubbles at Submerged Orifices," *AIChE J.*, Vol. 5, No. 3, pp. 319-324, (1956).

[5] S. Ramakrishnan, R. Kumar, and N. R. Kuloor, "Studies in bubble formation—I bubble formation under constant flow conditions," *Chem. Eng. Sci.*, Vol. 24, No. 4, pp. 731-747, (1969).

[6] K. Akita and F. Yoshida, "Gas Holdup and Volumetric Mass Transfer Coefficient in Bubble Columns. Effects of Liquid Properties," *Ind. Eng. Chem. Process Des. Dev.*, Vol. 12, No. 1, pp. 76-80, (1973).

[7] E. Sada, A. Yasunzshz, S. Katoh, and M. Nishioka, "Bubble Formation in Flowing Liquid," *Can. J. Chem. Eng.*, Vol. 56, No. 6, pp. 669-672, (1978).

[8] H. Tsuge and S.-I. Hibino, "Bubble Formation From an Orifice Submerged in Liquids," *Gordon Breach. Sci. Publ. Inc.*, Vol. 22, pp. 63-79, (1983).

[9] I. Kim, Y. Kamotani, and S. Ostrach, "Modeling bubble and drop formation in flowing liquids in microgravity," *AIChE J.*, Vol. 40, No. 1, pp. 19-28, (1994).

[10] A. Byakova, S. Gnyloskurenko, T. Nakamura, and O. . Raychenko, "Influence of wetting conditions on bubble formation at orifice in an inviscid liquid Mechanism of Bubble Evolution," *Colloids Surfaces A Physicochem. Eng. Asp.*, Vol. 229, No. 1-3, pp. 19-32, (2003).

[11] G. Corchero, a. Medina, and F. J. Higuera, "Effect of wetting conditions and flow rate on bubble formation at orifices submerged in water," *Colloids Surfaces A Physicochem. Eng. Asp.*, Vol. 290, No. 1-3, pp. 41-49, (2006).

[12] X. Qu and H. Qiu, "Bubble dynamics under a horizontal micro heater array," *J. Micromechanics Microengineering*, Vol. 19, No. 9, p. 095008, (2009).

[13] M. Ohta, Y. Yoshida, and M. Sussman, "A computational study of the dynamic motion of a bubble rising in Carreau model fluids," *Fluid Dyn. Res.*, Vol. 42, No. 2, p. 025501, (2010).

[14] S. Vafaei, P. Angeli, and D. Wen, "Bubble growth rate from stainless steel substrate and needle nozzles," *Colloids Surfaces A Physicochem. Eng. Asp.*, Vol. 384, No. 1-3, pp. 240-247, (2011).

[15] S. Di Bari and A. J. Robinson,

"Experimental study of gas injected bubble growth from submerged orifices," *Exp. Therm. Fluid Sci.*, Vol. 44, pp. 124-137, (2013).

[16] R. J. Benzing and J. E. Myers, "Low frequency bubble formation at horizontal circular orifices," *Ind. Eng. Chem.*, Vol. 47, No. 10, pp. 2087-2090, (1955).

[17] K. Terasaka and H. Tsuge, "Bubble formation under constant-flow conditions," *Chemical Engineering Science*, Vol. 48, No. 19. pp. 3417-3422, (1993).

[18] A. Zaruba, E. Krepper, H. M. Prasser, and B. N. Reddy Vanga, "Experimental study on bubble motion in a rectangular bubble column using high-speed video observations," *Flow Meas. Instrum.*, Vol. 16, No. 5, pp. 277-287, (2005).

[19] A. K. Das, P. K. Das, and P. Saha, "Formation of bubbles at submerged orifices - Experimental investigation and theoretical prediction," *Exp. Therm. Fluid Sci.*, Vol. 35, No. 4, pp. 618-627, (2011).

[20] N. Hooshyar, J. R. Van Ommen, P. J. Hamersma, S. Sundaresan, and R. F. Mudde, "Dynamics of single rising bubbles in neutrally buoyant liquid-solid suspensions," *Phys. Rev. Lett.*, Vol. 110, No. 24, pp. 2-5, (2013).

[21] S. B. Harvey, J. P. Best, and W. K. Soh, "Vapour bubble measurement using image analysis," *Meas. Sci. Technol.*, Vol. 7, No. 4, pp. 592-604, (1996).

[22] J. F. Davidson and B. O. G. Schüler, "Bubble formation at an orifice in a viscous liquid," *Chem. Eng. Res. Des.*, Vol. 75, pp. S105-S115, (1997).

[23] M. Iguchi, Y. Terauchi, and S. Yokoya, "Effect of Cross-Flow on the Frequency of Bubble Formation from a Single-Hole Nozzle," *Metall. Mater. Trans. B*, Vol. 29, No. December, pp. 1219-1225, (1998).

[24] V. K. Badam, V. Buwa, and F. Durst, "Experimental Investigations of Regimes Under Constant Flow Condition," *Can. J. Chem. Eng.*, Vol. 85, No. June, pp. 257-267, (2007).

[25] L. Zhang, C. Yang, and Z. S. Mao, "Unsteady motion of a single bubble in

highly viscous liquid and empirical correlation of drag coefficient," *Chem. Eng. Sci.*, Vol. 63, No. 8, pp. 2099-2106, (2008).

[26] P. Hanafizadeh, J. Eshraghi, E. Kosari, and W. H. Ahmed, "The Effect of Gas Properties on Bubble Formation, Growth and Detachment," *Part. Sci. Technol.*, Vol. 6351, No. November, p. 150407162559008, (2015).

[27] S. E. Hosseini-Doost, A. Sattari, P. Hanafizadeh, and M. Molaei, "A method for bubble volume measurement under constant flow conditions in gas – liquid two-phase flow," *Energy Equip. Syst.*, Vol. 6, No. 1, pp. 89-99, (2018).

[28] P. Hanafizadeh, A. Sattari, S. E. Hosseini-Doost, A. G. Nouri, and M. Ashjaee, "Effect of orifice shape on bubble formation mechanism," *Meccanica*, Vol. 53, No. 10, pp. 1-23, (2018).

[29] E. Lazar, B. Deblauw, N. Glumac, C. Dutton, G. Elliott, and A. Head, "A Practical Approach to PIV Uncertainty Analysis," in *27th AIAA Aerodynamic Measurement Technology and Ground Testing Conference*, No. July, pp. 1-22, (2010).

[30] P. Hanafizadeh, S. Ghanbarzadeh, and M. H. Saidi, "Visual technique for detection of gas–liquid two-phase flow regime in the airlift pump," *J. Pet. Sci. Eng.*, Vol. 75, No. 3-4, pp. 327-335, (2011).

[31] L. Zhang and M. Shoji, "Aperiodic bubble formation from a submerged orifice," *Chem. Eng. Sci.*, Vol. 56, No. 18, pp. 5371-5381, (2001).

[32] M. Ishii and N. Zuber, "Drag coefficient and relative velocity in bubbly, droplet or particulate flows," *AIChE J.*, Vol. 25, No. 5, pp. 843-855, (1979).

[33] *Ansys fluent12.0, Theory Guide*, No. January. ANSYS, Inc, (2009).

[34] E. S. Gaddis and A. Vogelpohl, "Bubble formation in quiescent liquids under constant flow conditions," *Chem. Eng. Sci.*, Vol. 41, No. 1, pp. 97-105, (1986).

[35] M. Jamialahmadi, M. R. Zehtaban, H. Muller-Steinhagen, A. Sarrafi, and J. M. Smith, "Study of bubble formation under

constant flow conditions," *Chem. Eng. Res. Des.*, Vol. 79, No. 5, pp. 523-532, (2001).